frontiers in Materials

ORIGINAL RESEARCH
published: 24 June 2021
doi: 10.3389/fmats.2021.678658

In-Situ Process and Simulation of High-Performance Piezoelectric-on-Silicon Substrate for SAW Sensor

Rui Ma[1], *Weiguo Liu*[2]*, *Xueping Sun*[2] *and Shun Zhou*[2]

[1]School of Microelectronics, Xidian University, Xi'an, China, [2]Laboratory of Thin Film Techniques and Optical Test, Xi'an Technological University, Xi'an, China

This paper studied the manufacturing process of Piezoelectric-on-Silicon (POS) substrate which integrates 128° *Y–X* Lithium niobate thin film and silicon wafer using Smart-Cut technology. The blistering and exfoliation processes of the He as-implanted LN crystal under different annealing temperatures are observed by the *in-situ* method. Unlike the conventional polishing process, the stripping mechanism of the Lithium niobate thin film is changed by controlling annealing temperature, which can improve the surface morphology of the peeling lithium niobate thin film. We prepared the 128° *Y–X* POS substrate with high single-crystal Lithium niobate thin film and surface roughness of 3.91 nm through Benzocyclobutene bonding. After simulating the surface acoustic wave (SAW) characteristics of the POS substrate, the results demonstrate that the Benzocyclobutene layer not only performs as a bonding layer but also can couple more vibrations into the LN thin film. The electromechanical coupling coefficient of the POS substrate is up to 7.59% in the Rayleigh mode when h_{LN}/λ is 0.3 and h_{BCB}/λ is 0.1. Therefore, as a high-performance substrate material, the POS substrate has proved to be an efficient method to miniaturize and integrate the SAW sensor.

Keywords: piezoelectric-on-silicon substrate, lithium niobate thin film, *in-situ* method, blistering, exfoliation, surface acoustic wave sensor

OPEN ACCESS

Edited by:
Lin Zhang,
Massachusetts Institute of Technology, United States

Reviewed by:
Wen Wang,
Chinese Academy of Sciences, China
Venu Gopal Madhav Annamdas,
Continental, Germany

***Correspondence:**
Weiguo Liu
wgliu@163.com

Specialty section:
This article was submitted to Smart Materials, a section of the journal Frontiers in Materials

Received: *10 March 2021*
Accepted: *05 May 2021*
Published: *24 June 2021*

Citation:
Ma R, Liu W, Sun X and Zhou S (2021) In-Situ Process and Simulation of High-Performance Piezoelectric-on-Silicon Substrate for SAW Sensor. Front. Mater. 8:678658. doi: 10.3389/fmats.2021.678658

INTRODUCTION

The SAW sensor is a crucial element in military and civil electrical systems, such as in communication, navigation, radars, electronic countermeasures, telecontrol, telemetric systems, etc. To realize miniaturization and integration in SAW sensor fabrication, it is necessary to have interdigital transducers (IDT) and the corresponding electronic circuit on one chip (Fu et al., 2014; Bauer et al., 2015; Dargis et al., 2020). Nowadays, most of the SAW sensors are made on the piezoelectric crystal, which brings about difficulties in the integration and miniaturization (Lu et al., 2013; Mimura et al., 2017). Using a multilayer structure to prepare the SAW sensor is considered one of the most promising techniques (Moulet et al., 2008; Maouhoub et al., 2016; Tian et al., 2016; Sun et al., 2019; Naumenko, 2020). Since the piezoelectric-on-silicon (POS) substrate bonds the piezoelectric thin film on a silicon wafer, this structure can efficiently reduce the SAW sensor's volume and weight (Abdolvand et al., 2008; Ali and Lee, 2016). Therefore, the development and optimization of the high-performance POS substrate process have become a research hotspot.

Lithium niobate ($LiNbO_3$, LN) is widely adopted in the preparation of SAW sensors due to its excellent piezoelectric properties. Several techniques are applied to fabricate LN single-crystal thin films, such as RF sputtering and sol-gel (Ishihara et al., 2003; Takahashi et al., 2004). However, the complex lattice structures in the LN crystal lead to lattice mismatching between the thin film and substrate, subsequently seriously affecting the quality of the epitaxial film. To address this problem, an emerging technique, known as "Smart-Cut," was introduced to acquire high-quality single-crystal LN thin film (Bruel, 1995; Bruel et al., 1997). This technology has proven to be very advantageous in preparing LN thin films on insulators (LNOI), which structure is similar to the POS substrate (Rabiei and Gunter, 2004; Poberaj et al., 2009; Poberaj et al., 2012; Ma et al., 2014; Wang et al., 2018; Luo et al., 2019; Michael et al., 2019).

The Smart-Cut technology transfers the peeled thin film onto a supporting substrate through bonding and crystal ion slicing. Some research groups have reported their efforts on the use of Smart-Cut technology to prepare POS substrates. The difference of the published work lies in the use of different bonding technology and surface treatment of the peeled piezoelectric thin film. Several studies on bonding technology that determine whether the thin film can be successfully transferred to the substrate have been reported. Au-Au bonding is mainly dedicated to Bulk Acoustic Resonator (BAR), where the Au layer acts as the embedded electrode (Ballandras et al., 2019). Direct bonding is very demanding on the wafer to have a surface roughness less than 0.5 nm (Pastureaud et al., 2007). Using the SiO_2 film as a middle layer is also an efficient bonding method. The LN's temperature coefficient of the frequency (TCF) can be compensated by the SiO_2 (Hori et al., 2010). The SiO_2 layer with high density is deposited on the LN substrate by plasma-enhanced chemical vapor deposition (PECVD). To reduce bond defects and strengthen the bond between the ion-sliced $LiNbO_3$ thin film and the SiO_2 layer, the surface roughness of SiO_2 should be polished to less than 1 nm. However, the required roughness is hard to achieve because a typical SiO_2 layer is 2 μm (Poberaj et al., 2012). By contrast, benzocyclobutene (BCB) bonding does not have restrictions on the surface roughness, and expensive equipment is not necessary. It has become an extremely attractive bonding solution due to the advantages of high bonding strength, low processing temperature, simple process, and so on (Shuai et al., 2018). On the other hand, the annealing temperature is another key parameter in the preparation of POS substrates, which is crucial to the smooth striping of the LN wafer. A high annealing temperature will lead to the peeled LN thin film showing parallel microcracks under thermal stress (Shuai et al., 2018), and low annealing temperature will make it so the lattice damage layer formed by the ions implantation in the LN crystal cannot be repaired. Apart from the above problems, the surface roughness of the LN thin film on the POS substrate also greatly affects the performance of the device in the preparation of the SAW sensor. However, there are few reports on how to improve the surface morphology of the peeled film. Chemical mechanical polishing (CMP) is one of the most commonly used polishing techniques, and it can reduce the root mean square (RMS) roughness of the LN thin film to 0.5 nm (Poberaj et al., 2012). However, the polishing of sub-micron thin films will increase internal stress and damage the LN thin film. Lately, some literature has reported using low-energy Ar^+ radiation as a non-contact polishing process to treat the thin film surface. When the kinetic energy of Ar^+ ions is very low, Ar^+ interacts with atoms on the surface of the LN thin film, reducing the RMS of the LN thin film from 10.81 to 4.66 nm (Luo et al., 2019). These methods all require additional polishing process steps. On the basis of ensuring performance, how to obtain higher performance POS substrates by optimizing process parameters or adopting simplified manufacturing processes is a valuable question that is worth further investigation.

In this study, the phenomena of blistering and exfoliation after ion implantation of the LN crystal were observed by *in-situ* method. Controlling the ion implantation conditions and annealing temperature can optimize the surface roughness of the stripped LN thin film. A 128° *Y–X* LN POS substrate with high-quality single crystal LN film and low surface roughness was prepared by BCB bonding. The SAW propagation characteristics of the 128° *Y–X* LN POS substrate were simulated by the finite element method (FEM).

EXPERIMENT

He ions were implanted into 2-inch 128° *Y–X* LN wafers under an energy of 200 keV. The implantation doses of He ions were 2.5×10^{16}, 4.0×10^{16}, and 6.0×10^{16} ions cm^{-2}. The LN wafers were implanted using LC-4 high-energy ion implantation equipment (Institute of semiconductors, Chinese academy of sciences). To minimize ion channeling, implantation was performed under a sample tilt of 7°. The LN wafers were cut into small pieces after ion implantation. The as-implanted LN samples were annealed in air at a temperature ranging from 30 up to 500°C. *In-situ* observation was carried out by optical microscope (DM2500, Leica) with a heating stage (THMS600, Linkam) and showed surface blistering and exfoliation. The as-implanted LN sample is bonded to the silicon wafer by BCB and annealed at a specific temperature. The morphology and surface roughness of the peeled LN thin film were measured with an atomic force microscope (AFM, Multimode8, Bruke).

The preparation process of the POS substrate by Smart-Cut technology is illustrated in **Figure 1**. The LN wafer was implanted with He ions, forming a damage layer with gaseous bubbles underneath the surface of the LN wafer. Flip the LN wafer. Next, the silicon (Si) sample was spin-coated with BCB (CYCLOTENE 3000, DOW Chemical Company), prebaking at 90°C for 3 min. The implanted surface of the LN sample and the Si wafer was then pre-bonded at 150°C for 10 min. Afterward, the LN sample/BCB/Si substrate pair was annealed in a vacuum. Eventually, the POS substrate with the LN thin film was completed. The surface of LN thin film was observed using an optical microscope. The crystalline quality of the stripping LN thin films was analyzed by X-ray diffraction (XRD) patterns. XRD was performed using a D8 Advance X-ray diffractometer. The POS structure and LN thin film thickness were estimated by field

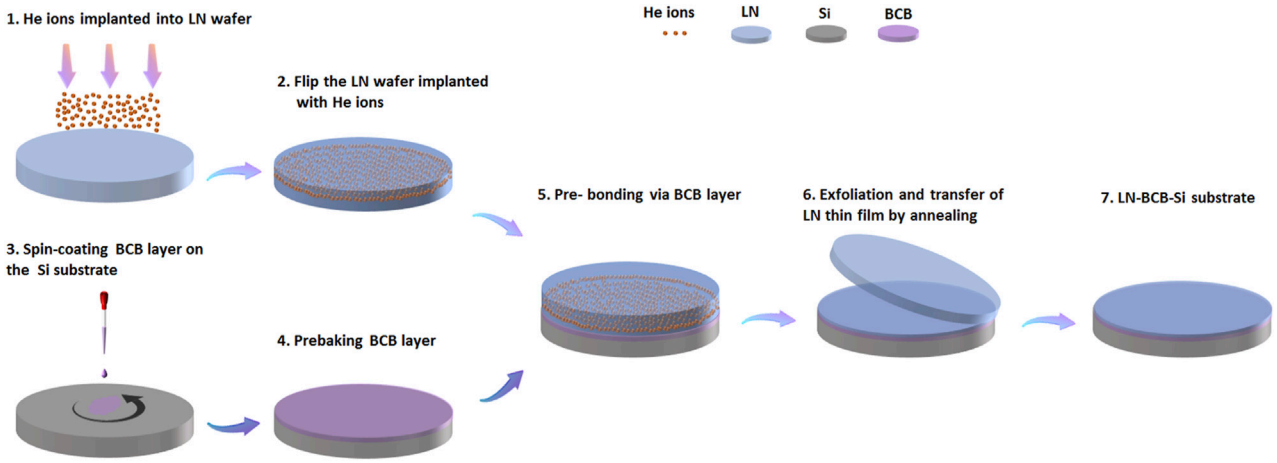

FIGURE 1 | The schematic drawing of POS substrate preparation process by smart-cut technology.

emission scanning electron microscope (FE-SEM, Zeiss GeminiSEM 500). The surface roughness of the LN thin film was measured by AFM.

RESULTS AND DISCUSSION

Blistering and Exfoliation of LN by *In-situ* Process

When He ions are implanted into the LN crystal, many nanometer-sized defects will be formed, called platelets. During the annealing process, He platelets grow laterally below the LN surface until they suddenly pop up as surface blisters due to the internal pressure after a critical size has been reached, causing blistering phenomenon (Huang et al., 1999). The time required to form optically detectable surface blisters for a given annealing temperature is termed blistering time. Since the blistering time and the annealing temperature are in accordance with the Arrhenius relationship, the change of annealing temperature has a very obvious influence on the blistering time (Tong et al., 1997). **Figure 2** shows the surface blistering of the 128° *Y–X* LN with an implantation energy of 200 KeV and a dose of 2.5×10^{16} ions cm^{-2} after annealing from 260 to 310°C. Under the same injection condition, it shows that the blistering time for the LN sample becomes shorter as the annealing temperature increases. **Figure 2A** indicates that blistering of the as-implanted LN sample started after 40 min under annealing at 260°C, while **Figure 2D** presents that blistering occurred after only heating 10 s under annealing at 310°C. Simultaneously, we have also observed that the as-implanted LN samples with the implantation dose of 2.5×10^{16} ions cm^{-2} will blister in the form of bubbles and grow larger until bubbles crack and strip off regardless of the annealing temperature.

Figure 3 presents the blistering and exfoliation phenomenon of 128° *Y–X* LN with an implantation energy of 200 KeV and a dose of 4.0×10^{16} ions cm^{-2} under annealing from 240 to 275°C. The as-implanted LN samples also comply with the rule that the higher the annealing temperature, the shorter the time for blistering. In addition, it can be seen from **Figure 3A** that obvious bubbles can be observed on the surface of the as-implanted LN sample after annealing at 240°C for 21 min. Extending annealing time, the density of bubbles on the sample surface increased significantly and the size of the bubbles also increased. Starting from 30 min, the surface of the sample was filled with bubbles, and some bubbles began to break. **Figure 3B** shows the blistering of the as-implanted LN surface annealing at 250°C. The large bubbles appeared on the surface of the LN sample within 14 min. At the 16th min, the density of the bubbles continued to increase. In addition to the small bubbles bursting, there were also larger-sized bubbles broken in the 21st min. Annealing at 260°C, **Figure 3C** shows that the surface of the LN sample blistered within 12 min. At the 19th min, the density of bubbles in the left area increased while some bubbles burst. Simultaneously, the large area of the LN thin film in the right area occurred exfoliation instead of blistering. After increasing the annealing temperature to 275°C, the LN did not blister, but exfoliation occurred directly, as shown in **Figure 3D**. Ion implantation formed plane defects, called "platelets," in the LN crystal. Platelets, acting as nucleation sites for the formation of microcracks are the origin of microcracks (Pang et al., 2012; Huang et al., 2019). In addition to lattice defects caused by implantation, strain and stress inside the crystal are also induced by ion implantation (Ofan et al., 2010). As the implantation up to a large dose of 4.0×10^{16} ions cm^{-2}, a high concentration of planar defects at the end of the ion range and large internal stress inside the LN crystal are formed. Therefore, under high-temperature annealing, gas-containing microcracks quickly propagate along the lateral direction. Due to the high concentration of the He platelets, the microcracks are easy to connect together on the same plane. In this way, large micro-cracks are formed, and regional exfoliation occurs along the domain wall. This is why the peeling presents a zigzag with regular edges. Based on the above research, the annealing temperature has a direct effect on the mechanism of blistering

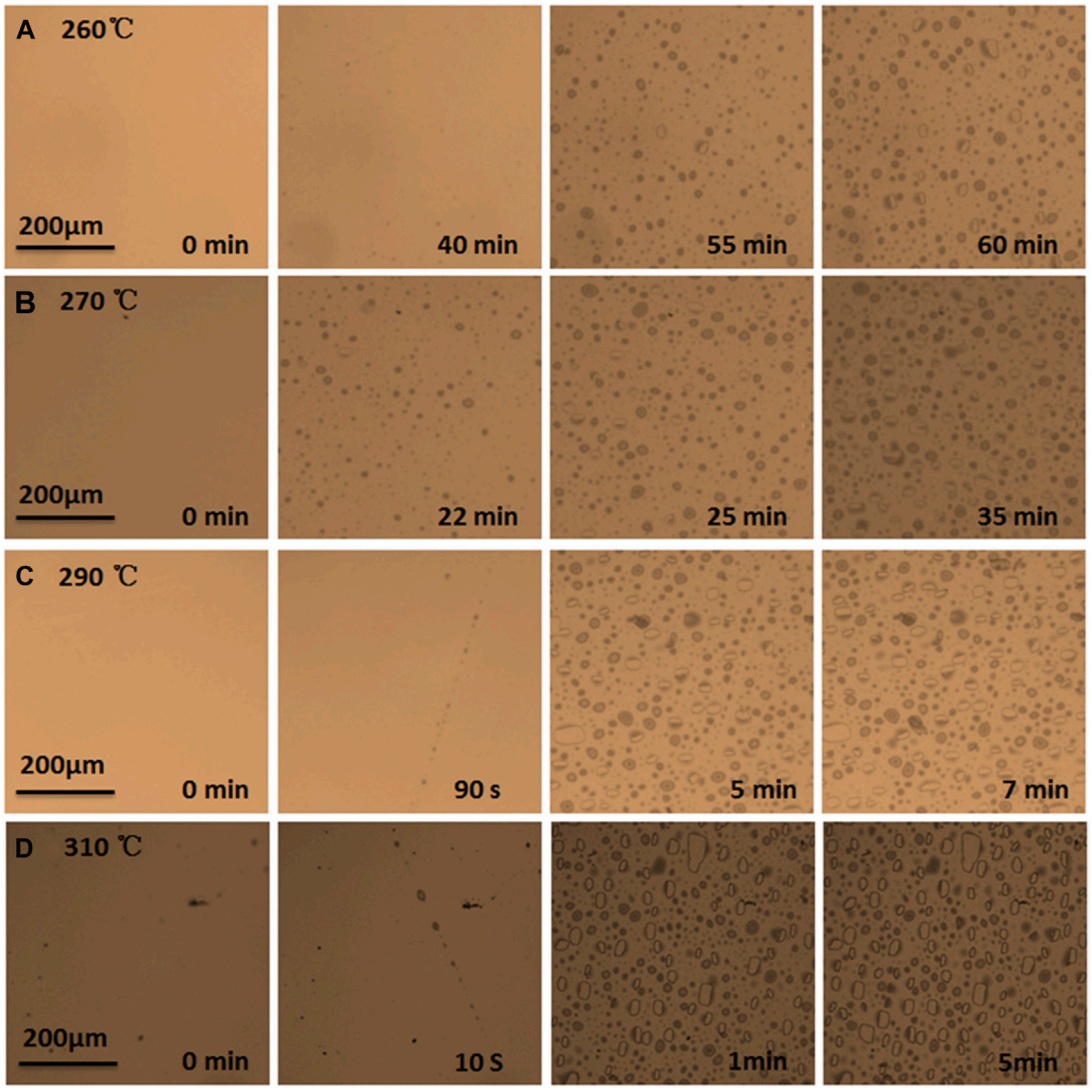

FIGURE 2 | Surface blistering of 128° *Y–X* LN implanted with a dose of 2.5 × 10^{16} ions cm^{-2} annealed at **(A)** 260°C, **(B)** 270°C, **(C)** 290°C, and **(D)** 310°C.

or exfoliation of LN crystal which implantation energy is 200 KeV and dose is 4.0 × 10^{16} ions cm^{-2}.

The residues after stripping were observed on the 128° *Y–X* LN sample surface with an implantation energy of 200 KeV and a dose of 6.0 × 10^{16} ions cm^{-2}, as shown in **Figure 4**. Notably, no blistering and exfoliation were observed on the as-implanted LN sample surface annealing from 30 to 500°C. It might be caused by the thermal effect generated during the ion implantation process. During ion implantation, the kinetic energy of He ions is transmitted to the target, and most of them are converted to thermal energy. The larger the implant dose means the more ions, the more heat it brings (Szafraniak et al., 2003; Ma et al., 2014). When the temperature of the LN sample caused by the thermal effect is higher than the blistering temperature, blistering or exfoliation will occur during the implantation process. Therefore, the temperature must be kept within a certain range, preferably at room temperature, during high-dose ion implantation.

For SAW sensors, the surface roughness of the piezoelectric thin film on the POS substrate will affect the performance of the IDT. Generally speaking, the surface of the LN thin film obtained by Smart-cut is relatively rough. The main reason for the large surface roughness of the LN thin film is that the He ion implantation into the LN crystal has a Gaussian distribution, and most of the bubbles generated during annealing are concentrated at its peak. Therefore, the thicknesses of the stripped LN thin films are not strictly equal. Base on the above research, we found that the 128° *Y–X* LN sample with an implantation energy of 200 KeV and a dose of 4.0 × 10^{16} ion cm^{-2} exhibited a large area of thin film exfoliation instead of blistering after 275°C. This stripped method inhibits the growth of bubbles in the vertical direction, accelerates the lateral spread of microcracks on the injection surface, and makes the LN thin film exfoliate in a large area. We measured the surface roughness of the stripped LN films obtained by blistering (at 240°C) and

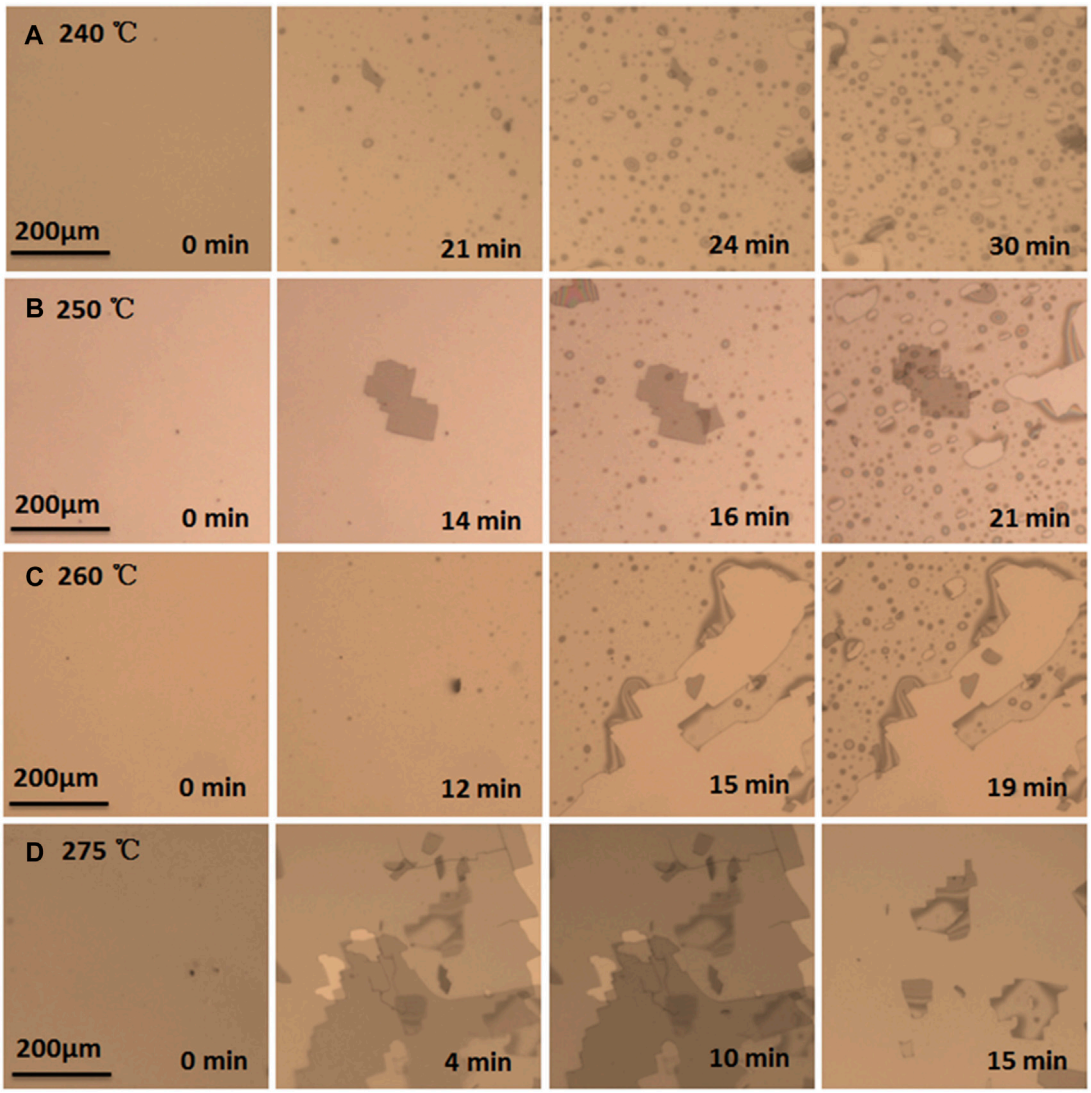

FIGURE 3 | Surface blistering of 128° *Y–X* LN implanted with a dose of 4.0 × 10^{16} ions cm^{-2} annealed at **(A)** 240°C, **(B)** 250°C, **(C)** 260°C, and **(D)** 275°C.

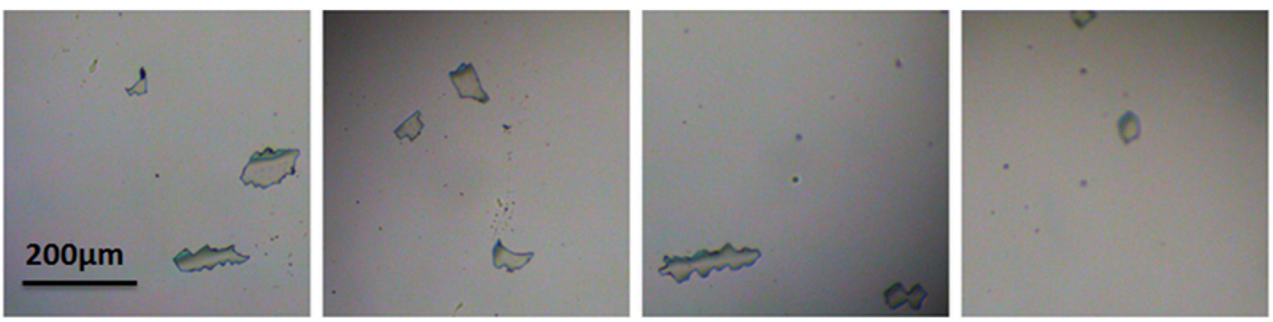

FIGURE 4 | The residues on the surface of as-implanted 128° *Y–X* LN with a He ions dose of 6.0 × 10^{16} ions cm^{-2}.

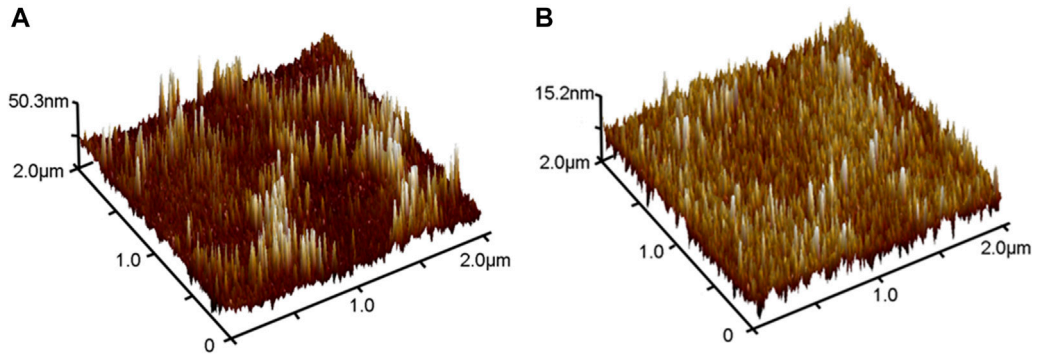

FIGURE 5 | AFM images of stripped LN thin films after annealing at **(A)** 240°C and **(B)** 275°C.

exfoliation (at 275°C) under the same injection conditions, respectively. As shown in **Figures 5A,B**, the RMS surface roughness of the LN film annealed at 240°C is 9.44 nm. By contrast, the RMS surface roughness of the LN film annealed at 275°C is as low as 3.89 nm. This result revealed that the surface roughness of the stripped LN thin film can be reduced by controlling the blistering or exfoliation method of the LN crystal after implantation.

Properties of POS Substrate

One of the aims of this work is to establish a POS substrate fabrication process using BCB bonding. The 128° *Y–X* LN with an implantation energy of 200 KeV and a dose of 4.0×10^{16} ions cm^{-2} was selected for the subsequent POS substrate fabrication. In the preparation process, annealing and bonding are crucial steps, which must be compatible with each other. After the as-implanted LN sample is bonded to a Si wafer that performs mechanical support in the following thermally induced splitting process. To achieve high-quality splitting, the bonding between the LN sample and Si wafer must be completed before the blistering of LN. Combine with the above investigation, the LN sample/BCB/Si substrate pair was annealed at 270°C for 2 h. The experimental steps of the POS substrate preparation are shown in **Supplementary Figure S1**. **Figure 6A** is an image of 128° *Y–X* LN POS substrate, which exhibits the LN thin film is exfoliated and transferred to the Si substrate. **Figure 6B** exhibits the cross-section of the 128° *Y–X* LN POS substrate with an LN thin film thickness of 692.2 nm and a BCB thickness of 3.082 μm. In the Smart-Cut technique, the thickness of exfoliated LN thin film is determined by the peak distribution of He ion implantation damage, which can be simulated using Stopping and Range of Ions in Matter (SRIM) software (Lim et al., 2020). **Figure 6C** shows the distribution of He ions and vacancies with 200 Kev implanted energy. The depth of the implanted He ions and vacancies are not strictly kept at the same level, but both followed Gaussian distribution. They are mostly gathered at a depth of 700–750 nm. Base on the thickness of LN thin films we obtained, it can be found that experimental results are consistent with the simulation results.

As shown in **Figure 7A**, the exfoliated LN thin film shows a flat surface without visible cracks or discontinuities. We take the lower annealing temperature to reduce the thermal stress in stripping of LN thin film. On the other hand, research has proved that high annealing temperature enables repairing the lattice damage which is induced by high energy ion implantation to some extent (Levy et al., 1998). Therefore, it is necessary to test the single crystalline of the LN thin film after low-temperature annealing. The XRD spectrum of the stripped LN thin film is shown in **Figure 7B**. Compared with the LN crystal standard card, the diffraction peaks of 128° *Y–X* LN thin film appear at 32.69° and 68.41°. The crystal planes are LN (104) and LN (208). The full width at half maximum (FWHM) of the LN (104) is 0.197°. The results indicate that the stripped LN thin film is a high-quality single-crystal thin film. **Figure 7C** shows the surface roughness of the 128° *Y–X* LN POS substrate, where the RMS roughness of the surface is 3.91 nm.

SAW Characteristics of POS Substrate

In addition to having smooth surface characteristics, the POS substrate is required to have as high an electromechanical coupling coefficient (K^2) as possible (Ro et al., 2009) to improve the energy conversion efficiency of the SAW sensor. The finite element analysis model is established to investigate the influence of structural parameters on SAW propagation characteristics in the POS substrate. In the multilayer structure, SAW propagation has dispersion characteristics and is related to the ratio of the thickness of the piezoelectric thin film to the SAW wavelength (El Hakiki et al., 2005). Taking 128° *Y–X* LN POS substrate as the simulation object, the model structure of IDT/LN/BCB/Si was established by COMSOL, as shown in **Supplementary Figure S2**. The detailed material constants are listed in **Supplementary Table S1** (Sun et al., 2019).

As shown in **Figures 8A,B**, the SAW phase velocity (v_p) and the K^2 of POS substrate are related to the normalized thickness of the LN thin film (h_{LN}/λ) and BCB layer (h_{BCB}/λ), where h_{LN} is the LN thin film thickness, h_{BCB} is the BCB layer thickness, λ is the SAW wavelength. The LN/Si structure without the BCB layer has been considered for comparison. The phase velocity is 3,980 m s^{-1} for the Rayleigh wave propagates in a 128° *Y–X* LN crystal (Tomar et al., 2001). The phase velocities of BCB and Si can be calculated from the Rayleigh wave equation in solids, which are 807 and 5,339 m/s, respectively (Zhou et al., 2013). Therefore, the Rayleigh mode equivalent phase velocity of the POS substrate should be between 807 and 5,339 m s^{-1}, and the

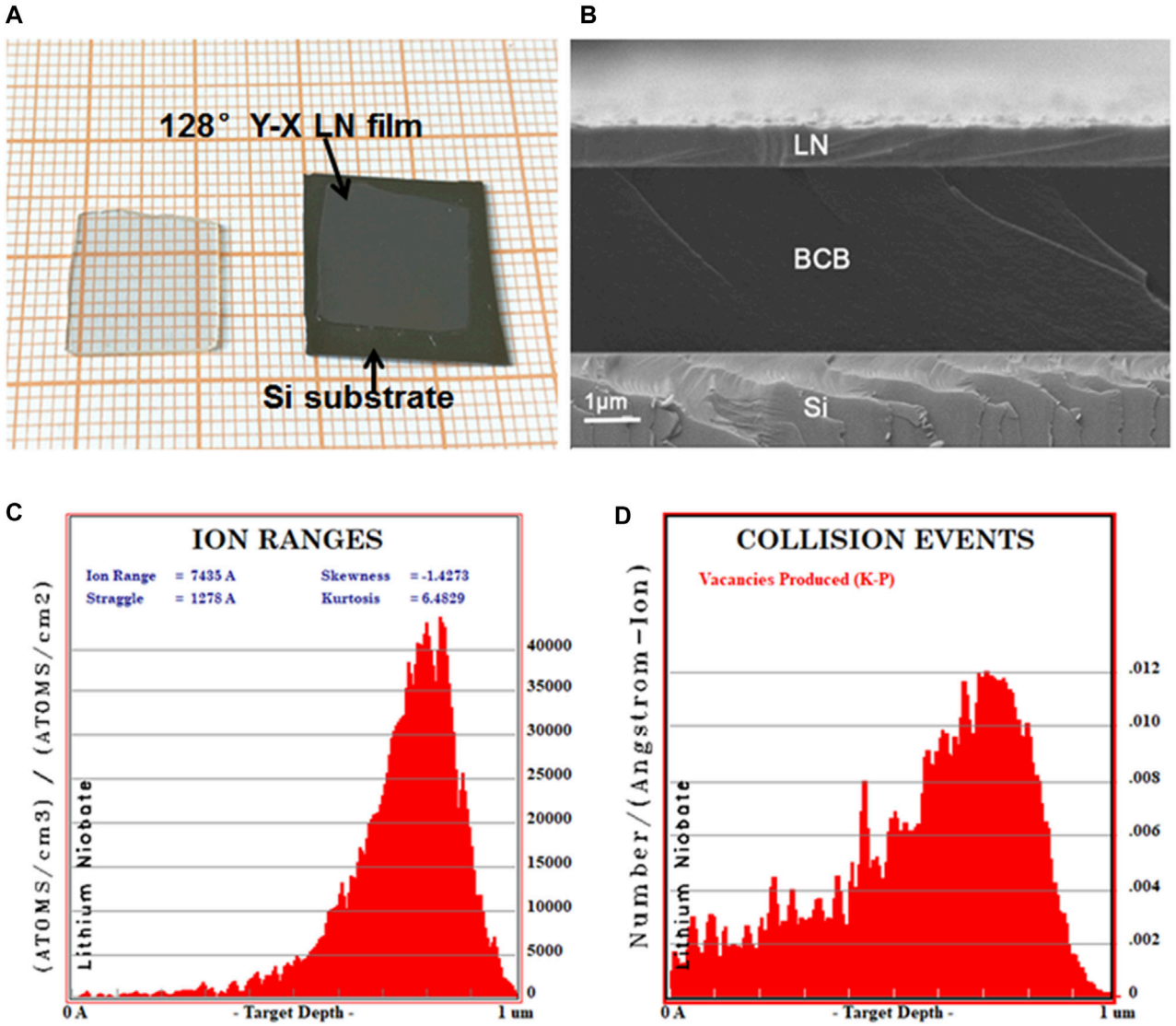

FIGURE 6 | (A) the photographs of 128° *Y–X* LN POS substrate, **(B)** The cross-section picture of 128° *Y–X* LN POS structure inspected by SEM, **(C)** He ions, and **(D)** vacancies distribution in LN crystal at 200 KeV implantation energy simulated by SRIM.

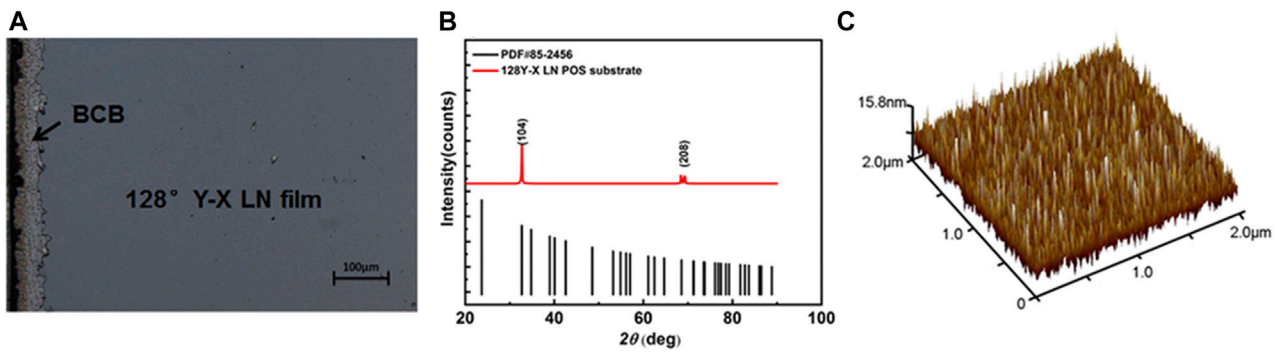

FIGURE 7 | (A) the optical microscopy images of the 128° *Y–X* LN POS substrate surface, **(B)** the XRD spectrum of the stripped LN thin film on the128° *Y–X* LN POS substrate, and **(C)** AFM images of the 128° *Y–X* LN POS substrate surface.

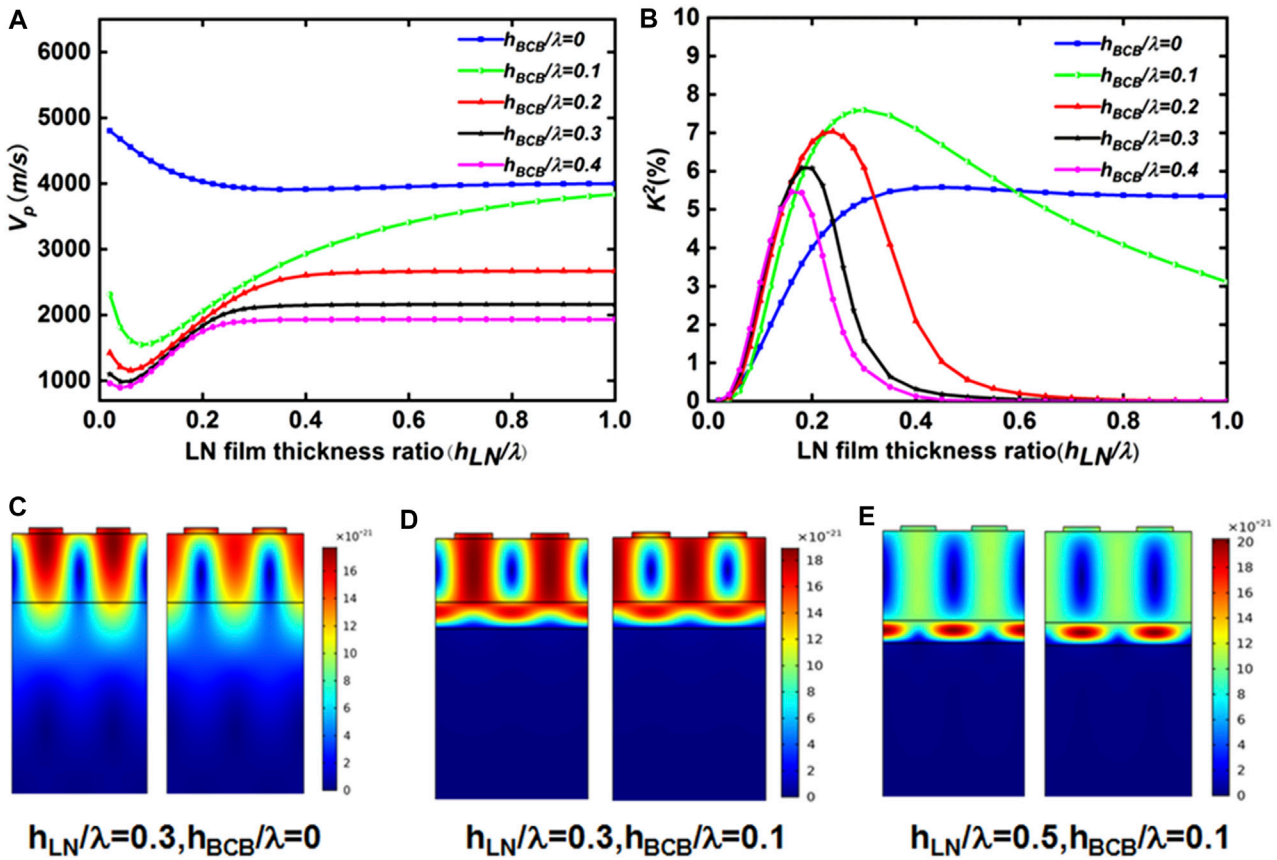

FIGURE 8 | (A) v_p dispersion curves and **(B)** K^2 dispersion curves of the 128° *Y–X* LN POS substrate, **(C)** vibration mode of POS substrates with h_{LN}/λ = 0.3 and h_{BCB}/λ = 0, **(D)** vibration mode of POS substrates with h_{LN}/λ = 0.3 and h_{BCB}/λ = 0.1, **(E)** vibration mode of POS substrates with h_{LN}/λ = 0.5 and h_{BCB}/λ = 0.1.

phase velocity of LN/Si structure is ranging from 3,980 to 5,339 m s^{-1}. Noticeable, only when h_{LN}/λ < 0.03 a*nd* h_{BCB}/λ < 0.05, the v_p of POS substrate is between 3,980 and 5,339 m s^{-1}, and the rest v_p are all between 807 and 3,980 m s^{-1}, which is confirmed by **Figure 8A**. The results demonstrate that the BCB layer has a significant effect on the v_p of POS substrate, which subsequently affects the center frequency of the SAW device. With a constant h_{BCB}/λ, the v_p of the POS substrate decreases rapidly with the thickness of the LN layer, becomes larger as h_{LN}/λ increases, and eventually remains constant when the depth reaches a specific value. When the thickness of the LN layer is constant, v_p decreases when h_{BCB}/λ increases. In **Figure 8B**, the K^2 of LN/Si structure rises with the rising h_{LN}/λ. When h_{LN}/λ > 0.3, the K^2 is approximately 5.3%, which is close to 128° *Y–X* LN crystal. When h_{BCB}/λ is constant, the K^2 of the POS substrate increases with the thickness of the LN thin film and presents an illustrative tendency to rise first and then decrease. Taking h_{BCB}/λ = 0.1 as an example, given h_{LN}/λ = 0.1, the K^2 of the POS substrate is only 1.8%, which is considered a smaller value. When h_{LN}/λ increases, the K^2 of the POS substrate increases. When h_{LN}/λ is 0.3, the K^2 of the POS substrate reaches up to 7.59%, which is higher than 5.5% of the 128° *Y–X* LN crystal (Tomar et al., 2001). When h_{LN}/λ > 0.3, the K^2 of the POS substrate dropped. The changing trend of K^2 in the POS substrate is related to its vibration mode. **Figures 8C–E** exhibit the vibration mode of POS substrates with different h_{LN}/λ and h_{BCB}/λ, respectively. When h_{LN}/λ is 0.3, h_{BCB}/λ is 0, the Rayleigh wave vibration is mainly concentrated in the LN layer, and there is also some vibration in the silicon layer. Therefore, the K^2 of the LN/Si structure is close to but not larger than the LN crystal. When h_{LN}/λ is 0.3, h_{BCB}/λ is 0.1, the Rayleigh wave's vibration is concentrated mostly in the piezoelectric thin film. Meanwhile, the vibration is restricted to the BCB layer, and there is no leaking in the Si layer. The BCB layer performs as a bonding layer and couples more SAW energy into the LN thin film. Therefore, the K^2 of the POS substrate is improved significantly. When h_{LN}/λ is 0.5, h_{BCB}/λ is 0.1, the vibration of the SAW started to concentrate on the BCB layer. The K^2 of the POS substrate has declined because the BCB does not have piezoelectric characteristics. The above simulation results indicated that the coupling effect of the BCB layer has a significant impact on the increasing of K^2 in a POS substrate under certain conditions. The thickness of the BCB layer is related to the speed of the spin coating. Moreover, LN thin films of different thicknesses can be obtained by controlling the implantation energy of He ions. Therefore, the performance of SAW propagation can be further improved by optimizing the POS structure parameters, which leads to a high-performance SAW sensor.

CONCLUSION

We proposed a preparation scheme for using Smart-Cut technology to manufacture high-quality POS substrates. Under different implantation conditions, either blistering or exfoliation of LN crystals during annealing is observed with the *in-situ* method. The results reveal the surface roughness of the peeled LN thin film can be improved by adjusting the annealing temperature. We applied BCB bonding to prepare the 128° *Y–X* LN POS substrate that proved to have good single-crystal properties and surface morphology. Compared with the LN/Si structure, the BCB layer in the POS substrate can concentrate more SAW vibration in the piezoelectric thin film layer according to the surface acoustic wave characteristics finite element analysis, which improves the K^2 of the POS substrate. When h_{LN}/λ is 0.3 and h_{BCB}/λ is 0.1, the K^2 of 128° *Y–X* LN POS substrate is as high as 7.59% in the Rayleigh mode. Overall, as a high-performance substrate material, the POS substrate is proved to be efficient in improving performance and reducing the size of the SAW sensor.

DATA AVAILABILITY STATEMENT

The original contributions presented in the study are included in the article/**Supplementary Material**, further inquiries can be directed to the corresponding author.

AUTHOR CONTRIBUTIONS

RM participated in ion implantation and annealing experiments, organized all the images and data, and fabricated the POS substrate; ZS participated in the acquisition of SEM, AFM images, and XRD data. XS participated in the simulation of POS substrate SAW characteristics and data discussion; WL proposed the study and was deeply involved in the discussion of the results and in the writing of the manuscript. All authors contributed to manuscript revision and approved the submitted version.

FUNDING

This research was supported by the National Basic Research Project (No. JCKY2016208A002), the Advanced Manufacturing Project (No. 41423020111), and the Advanced Research Fund Project (No. 6141B010271).

SUPPLEMENTARY MATERIAL

The Supplementary Material for this article can be found online at: https://www.frontiersin.org/articles/10.3389/fmats.2021.678658/full#supplementary-material

REFERENCES

Abdolvand, R., Lavasani, H., Ho, G., and Ayazi, F. (2008). Thin-film Piezoelectric-On-Silicon Resonators for High-Frequency Reference Oscillator Applications. *IEEE Trans. Ultrason. Ferroelect., Freq. Contr.* 55 (12), 2596–2606. doi:10.1109/TUFFC.2008.976

Ali, A., and Lee, J. E.-Y. (2016). "Square-extensional Mode Piezoelectric-On-Silicon Resonator for Physical Measurements of Liquids." in IEEE International Frequency Control Symposium (IFCS) (IEEE), 1–4. doi:10.1109/fcs.2016.7546823

Ballandras, S., Courjon, E., Bernard, F., Laroche, T., and Butaud, E. (2019). "New Generation of SAW Devices on Advanced Engineered Substrates Combining Piezoelectric Single Crystals and Silicon."in 2019 Joint Conference of the IEEE International Frequency Control Symposium an European Frequency and Time Forum (EFTF/IFC). doi:10.1109/fcs.2019.8855991

Bauer, T., Eggs, C., Wagner, K., and Hagn, P. (2015). A Bright Outlook for Acoustic Filtering: a New Generation of Very Low-Profile SAW, TC SAW, and BAW Devices for Module Integration. *IEEE Microwave* 16 (7), 73–81. doi:10.1109/MMM.2015.2429512

Bruel, M., Aspar, B., and Auberton-Hervé, A.-J. (1997). Smart-Cut: A New Silicon on Insulator Material Technology Based on Hydrogen Implantation and Wafer Bonding*1. *Jpn. J. Appl. Phys.* 36 (3S), 1636–1641. doi:10.1143/JJAP.36.1636

Bruel, M. (1995). Silicon on Insulator Material Technology. *Electron. Lett.* 31 (14), 1201–1202. doi:10.1049/el:19950805

Dargis, R., Clark, A., Ansari, A., Hao, Z., Park, M., Kim, D., et al. (2020). Single-Crystal Multilayer Nitride, Metal, and Oxide Structures on Engineered Silicon for New-Generation Radio Frequency Filter Applications. *Phys. Status Solidi A.* 217 (7), 1900813. doi:10.1002/pssa.201900813

El Hakiki, M., Elmazria, O., Assouar, M. B., Mortet, V., Le Brizoual, L., Vanecek, M., et al. (2005). ZnO/AlN/diamond Layered Structure for SAW Devices Combining High Velocity and High Electromechanical Coupling Coefficient. *Diamond Relat. Mater.* 14 (3-7), 1175–1178. doi:10.1016/j.diamond.2005.01.002

Fu, C., Elmazria, O., Sarry, F., Mahalingam, T., Yang, S. S., and Lee, K. (2014). Development of Wireless, Batteryfree Gyroscope Based on One-Port SAW Delay Line and Double Resonant Antenna. *Sens. Actuators A: Phys.* 220, 270–280. doi:10.1016/j.sna.2014.10.006

Hori, Y., Kobayashi, H., Tohyama, K., Iwasaki, Y., and Suzuki, K. (2010). "A Hybrid Substrate for a Temperature-Compensated Surface Acoustic Wave Filter,"in 2009 IEEE International Ultrasonics Symposium. doi:10.1109/ultsym.2009.5441626

Huang, K., Li, Z., Yan, Y., Zhao, X., Li, W., You, T., et al. (2019). Comparative Study of the Ion-Slicing Mechanism of Y-Cut LiNbO3. *AIP Adv.* 9 (8), 085001. doi:10.1063/1.5112792

Huang, L.-J., Tong, Q.-Y., Chao, Y.-L., Lee, T.-H., Martini, T., and Gösele, U. (1999). Onset of Blistering in Hydrogen-Implanted Silicon. *Appl. Phys. Lett.* 74 (7), 982–984. doi:10.1063/1.123430

Ishihara, M., Nakamura, T., Kokai, F., and Koga, Y. (2003). Preparation of Lithium Niobate Thin Films on diamond-coated Silicon Substrate for Surface Acoustic Devices. *Diam. Relat. Mater.* 12 (10-11), 1809–1813. doi:10.1016/s0925-9635(03)00212-7

Levy, M., Osgood, R. M., Liu, R., Cross, L. E., Cargill, G. S., Kumar, A., et al. (1998). Fabrication of Single-crystal Lithium Niobate Films by crystal Ion Slicing. *Appl. Phys. Lett.* 73 (16), 2293–2295. doi:10.1063/1.121801

Lim, C.-M., Zhao, Z., Sumita, K., Toprasertpong, K., Takenaka, M., and Takagi, S. (2020). Effects of Hydrogen Ion Implantation Dose on Physical and Electrical Properties of Ge-On-Insulator Layers Fabricated by the Smart-Cut Process. *AIP Adv.* 10 (1), 015045. doi:10.1063/1.5132881

Lu, X., Mouthaan, K., and Soon, Y. T. (2014). Wideband Bandpass Filters with SAW-filter-like Selectivity Using Chip SAW Resonators. *IEEE Trans. Microwave Theor. Techn.* 62 (1), 28–36. doi:10.1109/TMTT.2013.2292041

Luo, W., Luo, J., Shuai, Y., Zhang, K., Wang, T., Wu, C., et al. (2019). Infrared Detector Based on crystal Ion Sliced LiNbO3 Single-crystal Film with BCB Bonding and thermal Insulating Layer. *Microelectronic Eng.* 213, 1–5. doi:10.1016/j.mee.2019.04.004

Ma, C., Lu, F., and Ma, Y. (2014). Blistering and Cracking of LiTaO3 Single crystal under Helium Ion Implantation. *Appl. Phys. A.* 118 (4), 1233–1238. doi:10.1007/s00339-014-8821-5

Maouhoub, S., Aoura, Y., and Mir, A. (2016). FEM Simulation of AlN Thin Layers on diamond Substrates for High Frequency SAW Devices. *Diamond Relat. Mater.* 62, 7–13. doi:10.1016/j.diamond.2015.12.004

Michael, R., Peter, O., Weigel, J., Zhao, J., and Mookherjea, S. (2019). Toward 3D Integrated Photonics Including Lithium Niobate Thin Films: A Bridge between Electronics, Radio Frequency, and Optical Technology. *Nanotechnol. Mag. IEEE* 13 (4), 18–33. doi:10.1109/MNANO.2019.2916115

Mimura, M., Ajima, D., Konoma, C., and Murase, T. (2017). "Small Sized Band 20 SAW Duplexer Using Low Acoustic Velocity Rayleigh SAW on $LiNbO_3$ Substrate,IEEE International Ultrasonics Symposium (IUS) (IEEE), 1–4. doi:10.1109/ultsym.2017.8092581

Moulet, J., Pijolat, M., Dechamp, J., Mazen, F., Tauzin, A., Rieutord, F., et al. (2008). "High Piezoelectric Properties in $LiNbO_3$ Transferred Layer by the Smart Cut™ Technology for Ultra Wide Band BAW Filter Applications," in 2018 IEEE International Electron Devices Meeting, 1–4. doi:10.1109/iedm.2008.4796785

Naumenko, N. F. (2020). Advanced Substrate Material for SAW Devices Combining $LiNbO_3$ and Langasite. *IEEE Trans. Ultrason. Ferroelect., Freq. Contr.* 67 (9), 1909–1915. doi:10.1109/TUFFC.2020.2985744

Ofan, A., Zhang, L., Gaathon, O., Bakhru, S., Bakhru, H., Zhu, Y., et al. (2010). Publisher's Note: Spherical Solid He Nanometer Bubbles in an Anisotropic Complex Oxide [Phys. Rev. B82, 104113 (2010)]. *Phys. Rev. B* 82 (10), 2511–2524. doi:10.1103/PhysRevB.82.109901

Pang, L. L., Wang, Z. G., Jin, Y. F., Yao, C. F., Cui, M. H., Sun, J. R., et al. (2012). The Modification of LiTaO3 crystal by Low-Energy He-Ion Implantation. *Nucl. Instr. Methods Phys. Res. Section B: Beam Interactions Mater. Atoms* 290 (none), 54–58. doi:10.1016/j.nimb.2012.09.003

Pastureaud, T., Solal, M., Biasse, B., Aspar, B., Briot, J.-B., Daniau, W., et al. (2007). High-frequency Surface Acoustic Waves Excited on Thin-Oriented LiNbO/sub 3/Single-crystal Layers Transferred onto Silicon. *IEEE Trans. Ultrason. Ferroelect., Freq. Contr.* 54 (4), 870–876. doi:10.1109/tuffc.2007.321

Poberaj, G., Hu, H., Sohler, W., and Günter, P. (2012). Lithium Niobate on Insulator (LNOI) for Micro-photonic Devices. *Laser Photon. Rev.* 6 (4), 488–503. doi:10.1002/lpor.201100035

Poberaj, G., Koechlin, M., Sulser, F., Guarino, A., Hajfler, J., and Günter, P. (2009). Ion-sliced Lithium Niobate Thin Films for Active Photonic Devices. *Opt. Mater.* 31 (7), 1054–1058. doi:10.1016/j.optmat.2007.12.019

Rabiei, P., and Gunter, P. (2004). Optical and Electro-Optical Properties of Submicrometer Lithium Niobate Slab Waveguides Prepared by crystal Ion Slicing and Wafer Bonding. *Appl. Phys. Lett.* 85 (20), 4603–4605. doi:10.1063/1.1819527

Ro, R., Chiang, Y. F., Sung, C. C., Lee, R., and Wu, S. (2009). Theoretical Analysis of SAW Propagation Characteristics in (100) Oriented AlN/diamond Structure. *IEEE Trans. Ultrason. Ferroelectr Freq Control.* 57 (1), 46–51. doi:10.1109/TUFFC.2010.1377

Shuai, Y., Gong, C., Bai, X., Wu, C., Luo, W., Böttger, R., et al. (2018). Fabrication of Y128- and Y36-Cut Lithium Niobate Single-Crystalline Thin Films by crystal-ion-slicing Technique. *Jpn. J. Appl. Phys.* 57 (4S), 04FK05. doi:10.7567/jjap.57.04fk05)

Sun, X., Liu, W., Ge, S., Zhou, S., Li, X., and Lin, D. (2019). Achieving Both High Electromechanical Response and Stable Temperature Behavior in Si/SiO2/Al/LiTaO3 sandwich Structure. *AIP Adv.* 9 (3), 035145. doi:10.1063/1.5083128

Szafraniak, I., Radu, I., Scholz, R., Alexe, M., and Gösele, U. (2003). Single-Crystalline Ferroelectric Thin Films by Ion Implantation and Direct Wafer Bonding. *Integrated Ferroelectrics* 55 (1), 983–990. doi:10.1080/10584580390259452

Takahashi, M., Yamauchi, K., Yagi, T., Nishiwaki, A., Wakita, K., Ohnishi, N., et al. (2004). Preparation and Characterization of High-Quality Stoichiometric LiNbO3 Thick Films Prepared by the Sol-Gel Method. *Thin Solid Films* 458 (1-2), 108–113. doi:10.1016/j.tsf.2003.12.066

Tian, X.-G., Tao, L.-Q., Liu, B., Zhou, C., Yang, Y., and Ren, T.-L. (2016). Surface Acoustic Wave Devices Based on High Quality Temperature-Compensated Substrates. *IEEE Electron. Device Lett.* 37 (8), 1063–1066. doi:10.1109/LED.2016.2584785

Tomar, M., Gupta, V., Mansingh, A., and Sreenivas, K. (2001). Temperature Stability Ofc-axis Oriented LiNbO3/SiO2/Si Thin Film Layered Structures. *J. Phys. D: Appl. Phys.* 34 (15), 2267–2273. doi:10.1088/0022-3727/34/15/305

Tong, Q.-Y., Gutjahr, K., Hopfe, S., Gösele, U., and Lee, T.-H. (1997). Layer Splitting Process in Hydrogen-Implanted Si, Ge, SiC, and diamond Substrates. *Appl. Phys. Lett.* 70 (11), 1390–1392. doi:10.1063/1.118586

Wang, C., Zhang, M., Chen, X., Bertrand, M., Shams-Ansari, A., Chandrasekhar, S., et al. (2018). Integrated Lithium Niobate Electro-Optic Modulators Operating at CMOS-Compatible Voltages. *Nature* 562 (7725), 101–104. doi:10.1038/s41586-018-0551-y

Zhou, J., He, X., Jin, H., Wang, W., Feng, B., Dong, S., et al. (2013). Crystalline Structure Effect on the Performance of Flexible ZnO/polyimide Surface Acoustic Wave Devices. *J. Appl. Phys.* 114 (4), 044502. doi:10.1063/1.4816002

Conflict of Interest: The authors declare that the research was conducted in the absence of any commercial or financial relationships that could be construed as a potential conflict of interest.

Copyright © 2021 Ma, Liu, Sun and Zhou. This is an open-access article distributed under the terms of the Creative Commons Attribution License (CC BY). The use, distribution or reproduction in other forums is permitted, provided the original author(s) and the copyright owner(s) are credited and that the original publication in this journal is cited, in accordance with accepted academic practice. No use, distribution or reproduction is permitted which does not comply with these terms.